Consensus Control for Energy Storage Systems

Javad Khazaei, *Member, IEEE,* Zhixin Miao, *Senior Member, IEEE*

***Abstract*—In this paper, consensus integral control is applied for energy storage in microgrids to synchronize the state-of-charge (SoC) and power levels of batteries with limited information exchange. Both local information (SoC and power level) and neighbors' information (SoC and power level) will be fed into an integral control installed at every battery converter. The design is based on consensus control and takes into consideration of real-world battery coordination requirements, e.g., all batteries should work in the same charging or discharging mode. Compared with the consensus control in the existing literature for voltage consensus or battery SoC/power consensus, this paper offers a simple design. The major assumption of the paper is that each converter should possess an integral control. This assumption is valid since indeed integral controls exist if converters are equipped with secondary frequency control. The designed consensus control is validated by simulations on 14-bus microgrid and IEEE 57-bus power system. Simulation results demonstrate the effectiveness of the consensus integral control for variety modes of operation: charging, discharging, and load variation.**

NOMENCLATURE

E_i	Energy of i^{th} battery.
P_i	Power of i^{th} battery.
u_i	Consensus input for i^{th} battery.
L	Laplacian matrix of communication graph.
D	In degree matrix of communication graph.
A	Adjacency matrix of communication graph.
a_{ij}	Element ij of the adjacency matrix.
T	Transpose of a matrix.
x_i	State of the i^{th} system or agent.
c	Positive scalar coupling gain.
K	Feedback control matrix variable.
R	Positive definite matrix in Riccati equation.
Q	Positive definite matrix in Riccati equation.
P_1	Positive definite solution of Riccati equation.
λ_i	Eigenvalues of laplacian matrix L.
$\otimes$	Kronecker product of two matrices.
C_c	Battery capacity in Farad.
V_n	Nominal battery voltage.
$f_1,\ f_2$	Correction factors in battery design.
V_{SOC}	State of charge voltage.
R_s	Battery series resistor.
R_{SD}	Battery self discharge resistor.
$R_{TS},\ R_{TL}$	Battery short and long transient resistors.
$C_{TS},\ C_{TL}$	Battery short and long transient capacitors.
P^*	Battery initial reference.
$P_{\rm ref}$	Battery final reference including consensus control.
ω_0	Reference frequency of the system.
ω	Measured frequency of the system.
R_f	Droop gain for the active power controller.
R_q	Droop gain for the reactive power controller.
$V_{\rm ref}$	Magnitude of the reference voltage.
T_i	The i^{th} Transformer.

***Index Terms*—Battery Energy Storage System, Consensus Control, Double Integrator, Microgrid, Secondary Control.**

I. INTRODUCTION

Microgrid technology provides an effective solution to integrate renewable energy sources, loads and energy storage systems. This paper focuses on coordination of batteries to achieve SoC and power level consensus through distributed consensus control.

Motivation: One of the most significant concerns related to the renewable energy sources in the microgrids is their limited operating times due to the uncertain behavior. For example, Photovoltaic (PV) modules can only generate electricity in presence of sun irradiance [1, 2], or wind farms can only operate in places where the sufficient amount of wind exists [3]. Battery energy storage systems are commonly implemented as the energy buffers [4–6]. There are a lot of examples that energy storages are used in microgrids to cooperate with the renewable energy sources [5, 7]. For example, [5] studies the smoothing performance of PV and wind generation in presence of battery energy storage systems as a hybrid microgrid.

Although the battery energy storage system can help the operation of renewable energy sources in the microgrids, its operation is not limited to a single task. Similar as traditional power systems, hierarchical control has been implemented in microgrids. Hierarchial control of energy storage system is a recently proposed topic which enables the energy storage system with multi-task operation capabilities [8–12].

Centralized and decentralized controllers are two main approaches in hierarchical control design for microgrids. A centralized controller manages a large amount of data, which are vulnerable to a single point of failure. Decentralized and distributed control structures have recently been proposed to enhance reliability for microgrid control. The main purpose of distributed cooperative control is to achieve a general agreement among all control agents with limited data transfer. Furthermore, in case of communication system failure or physical system failure, the entire system will not shut down. It only will effect the faulted elements. Distributed control based on consensus theory for network of dynamic agents was introduced in 2003 [13]. It was then applied to the mobile networks [14], sensor fusion and motion estimation [15]. The application of consensus theory in power systems is fairly new. Application of consensus can be found in power system economic dispatch [16–18] and microgrid control [19–22].

Related work: Distributed control has been proposed for secondary control in microgrids [19–22]. For example, [20]

J. Khazaei is with the school of science, engineering, and technology at Penn State Harrisburg, and Z. Miao is with the department of electrical engineering at University of South Florida, Tampa, FL (Email: zmiao@usf.edu)

proposes a feedback linearization based consensus control design for inverters in islanded microgrids. Consensus control is used to synchronize the inverter voltages. As another example, [21] proposes a consensus based droop control for real and reactive power sharing in microgrids. Consensus control has also been applied in battery converters to achieve consensus of SoC and power level [23–25].

Consensus SoC and power level is desirable among energy storage systems since such condition maintains high efficiency and state of health (SoH). With power and energy consensus, no single energy storage tends to go outside the allowed limit during the operating mode change. Therefore, the power capacity of the energy storage is maximized during the operation.

Both [23, 24] utilize high-order models (14 orders in [23] and 4 orders in [24]) to synthesize the consensus control input.

In [25], an average consensus algorithm is used to calculate the average SoC of the system and each battery will then follow that average SoC. This design needs global information and assumes a centralized center available.

Among all the mentioned references, general assumption is that the energy storage devices are working in one operating mode (islanded mode) and if the operating mode changes, the design needs to be changed as well. The previous distributed design [23, 24] is based on the following assumptions. (i) Each battery has exactly the same control architecture and control parameters. (ii) All states including SoC, power, current and voltage of a battery (e.g., [23]) will reach consensus. These two assumptions are very restrictive. Batteries may have different control architectures and parameters. There is also no need to require all states (including currents and voltages) to achieve consensus. The consensus design in [23] is based on a very complicated model for a specific control architecture and specific operation mode. Such design is be applicable if the operation mode of a microgrid is changed from autonomous to grid-connected.

Contribution: The objective of this research is to realize consensus SoC and power level for batteries in a microgrid. The designed approach will guarantee limited information exchange for both islanded and grid connected mode.

The design proposed in this paper is based on a simple second-order analytic model relating battery SoC and power with a control input. The outcome of the design is a simple distributed control architecture with only SoC and power as the exchanging information among agents. This control design is applicable in any operating modes: autonomous or grid-connected.

The function of the consensus control is to adjust power orders of batteries to achieve SoC/power consensus, while keeping the total power from batteries constant. In that sense, consensus control alone cannot bring system's frequency back to nominal. Therefore, similar as an area control error (ACE) signal in synchronous generators, this consensus input signal is combined with frequency deviation. The combined signal then will be sent to an integrator to generate the power order for each battery converter. This design combines consensus control with secondary frequency control. When the system has a load change, the proposed control can bring system frequency back to the nominal value and keep the battery SoC/power consensus. The proposed control is validated by simulation of a high fidelity 14-bus microgrid model built in OPAL's RT-LAB and IEEE 57-bus model in MATLAB.

The rest of the paper is as follows. Control design philosophy is presented in Section II. Validation test bed is described in Section III. RT-LAB simulation results are presented in Section IV. Section V includes the simulation results for IEEE 57-bus case. Section VI concludes the paper.

II. Consensus Design Philosophy

This objective of this problem is to achieve consensus for battery SoC and battery power. Though a few papers [23, 24] have been written on this subject, insights of consensus control are lost due to the complicated models. In addition, few papers adopt integral control to realize consensus. The foremost assumption is that the power order of a battery is generated through an integrator. Further, each converter has an integrator. Secondary frequency control uses integrator and this integrator can also be used for power and energy consensus.

Consensus control will be designed to be much slower than frequency control. Therefore, when there is a load change, frequency control quickly increases or decreases the total power to match the load. Afterwards, consensus control adjusts power among batteries, while keeping the total power constant.

A. System model and communication graph

Consider a communication graph of a system as shown in Fig. 1. There is a two-way communication link between the batteries. This graph can be represented by a Laplacian matrix L.

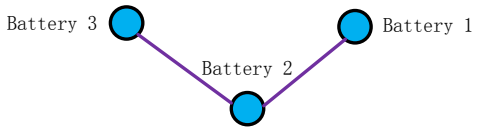

Fig. 1. Communication graph of the proposed system.

$$L = \begin{bmatrix} 1 & -1 & 0 \\ -1 & 2 & 1 \\ 0 & -1 & 1 \end{bmatrix} = \underbrace{\begin{bmatrix} 1 & 0 & 0 \\ 0 & 2 & 0 \\ 0 & 0 & 1 \end{bmatrix}}_{D} - \underbrace{\begin{bmatrix} 0 & 1 & 0 \\ 1 & 0 & 1 \\ 0 & 1 & 0 \end{bmatrix}}_{A} \quad (1)$$

where $L_{ij} = -a_{ij}, i \neq j$ and $a_{ij} > 0$, when i is connected with j and $a_{ij} = 0$ when i is not connected to j, $L_{ii} = \sum_{j \neq i} a_{ij}$, D is a diagonal matrix with diagonal elements representing the degree of each node, and A is a non-negative matrix with diagonal components zero.

The Laplacian matrix L has a trivial eigenvalue 0 with the corresponding right eigenvector of $\mathbf{1}$, a column vector with every element as 1.

$$L\mathbf{1} = 0 \quad (2)$$

For balanced graphs like the one in Fig. 1, L is a symmetric matrix, therefore,

$$\mathbf{1}^T L = (L\mathbf{1})^T = 0 \quad (3)$$

B. Design of the inputs

To make the design process easier, it is assumed that the battery energy storage can track the reference power very fast and accurate. Moreover, in islanded mode operation, it is assumed that the frequency controllers can quickly restore the frequency to its nominal value. Therefore, dynamics of the inner loops, secondary frequency control, and power controllers are neglected in this case. This will simplify the design.

The dynamics of each battery energy storage system can be written as:

$$\underbrace{\begin{bmatrix}\dot{E}_i\\ \dot{P}_i\end{bmatrix}}_{\dot{x}_i} = \underbrace{\begin{bmatrix}0 & -1/3600\\ 0 & 0\end{bmatrix}}_{A}\underbrace{\begin{bmatrix}E_i\\ P_i\end{bmatrix}}_{x_i} + \underbrace{\begin{bmatrix}0\\ 1\end{bmatrix}}_{B} u_i \tag{4}$$

where A, B are state matrices of the system, and E_i and P_i are energy and power for each battery. Since batteries use kWh and kW as the units for energy and power, in the time scale of seconds, a $1/3600$ coefficient is applied. A battery's per unit energy is the same as its state-of-charge (SoC) if the energy base is the same as the battery capacity.

For linear interconnected systems, consensus control design can be based on Lyapunov design, or optimal control design [26]. In this paper, optimal control design [27] is adopted. The dynamic model of each energy storage is represented as a state space model ($\dot{x}_i = Ax_i + Bu_i$).

The final goal of synchronization can be achieved if the power and energy difference between the neighbors is sent to each battery energy storage as a controller input. It is also noted that the $x = [x_1, x_2, ..., x_n]^T$ is a global vector of state variables, and $u = [u_1, u_2, ..., u_n]^T$ is the global vector of inputs in the system. The control input is designed as [20]:

$$u_i = cK\sum_{j=1}^{n} a_{ij}(x_j - x_i) = cK\sum_{j=1}^{n} a_{ij}\begin{bmatrix}E_j - E_i\\ P_j - P_i\end{bmatrix} \tag{5}$$

where a_{ij} is the element of the matrix A in (1), c is a positive scalar coupling gain, and K is the feedback control matrix variable.

The vector of all the inputs can be expressed as:

$$u = cL\begin{bmatrix}Kx_1\\ \vdots\\ Kx_n\end{bmatrix} \tag{6}$$

Therefore,

$$\sum_{i=1}^{n} u_i = \mathbf{1}^T u = c\mathbf{1}^T L\begin{bmatrix}Kx_1\\ \vdots\\ Kx_n\end{bmatrix} = 0 \tag{7}$$

Remarks: This is an important characteristic of consensus control. The sum of inputs are always 0. This also means that, the sum of power orders of all batteries should be constant. The function of the consensus control is to adjust power from each battery while keeping the total power constant. This function can be combined with secondary frequency control. When there is a load change, the secondary frequency control will take care of the load change by changing the power orders of each battery. The consensus control then maintains the sum of the power orders and adjusts individual power order to achieve consensus.

To properly select the gains, K can be found using linear quadratic regulator (LQR) design. Given two matrices Q and R as positive definite, the feedback gain K in (5) can be designed as [13, 20]:

$$K = R^{-1}B^T P_1 \tag{8}$$

where P_1 is the unique positive definite solution of the control algebraic Riccati equation (ARE) [13, 20]:

$$A^T P_1 + P_1 A + Q - P_1 B R^{-1} B^T P_1 = 0 \tag{9}$$

C. Stability

In order to analyze the stability of the proposed design, the closed-loop system dynamics should be considered. Adding the designed control input (5) into the state-space model of each agent leads to (10).

$$\dot{x_i} = Ax_i + cBK\sum_{j=1}^{n} a_{ij}(x_j - x_i) \tag{10}$$

The overall global closed-loop system can be represented as (11):

$$\dot{x} = (I_n \otimes A)x - cL \otimes BKx \tag{11}$$

[27] gives the stability criteria for the interconnected system which combines the control design requirements with the graph properties. If the eigenvalues of the Laplacian graph matrix L are denoted as λ_i, the stability properties of the global system dynamics in (11) is equivalent to the stability properties of:

$$\dot{z}_i = (A - \lambda_i cBK)z_i \qquad i = 1, 2, ..., n \tag{12}$$

The stability criterion requires $(A - \lambda_i cBK)$ to be Hurwitz, or all of its eigenvalues have a strictly negative real part. A sufficient condition requires c to be selected as [20]:

$$c = \max\left(\frac{1}{2\min Re(\lambda_i)}, 1\right) \qquad i = 2, ..., n \tag{13}$$

The proof and detailed discussion of the above stability criterion and the sufficient condition are provided in [28].

D. Numerical example

For a system with three energy storage units, given R and Q and solving for the Riccati equation in (9) provides matrix P. The control input K can be selected referring to (8) as $K = [K_1 \quad K_2]$ and c can be selected as (13) to be 1. The designed controller will be input to the battery energy storage in order to synchronize the energy levels. Considering the communication graph of the system shown in Fig. 1, three inputs can be selected as:

$$
\begin{aligned}
u_1 &= -c[K_1 \quad K_2]\begin{bmatrix} E_1 - E_2 \\ P_1 - P_2 \end{bmatrix} \\
u_2 &= -c[K_1 \quad K_2]\begin{bmatrix} 2E_2 - E_1 - E_3 \\ 2P_2 - P_1 - P_3 \end{bmatrix} \\
u_3 &= -c[K_1 \quad K_2]\begin{bmatrix} E_3 - E_2 \\ P_3 - P_2 \end{bmatrix}
\end{aligned} \tag{14}
$$

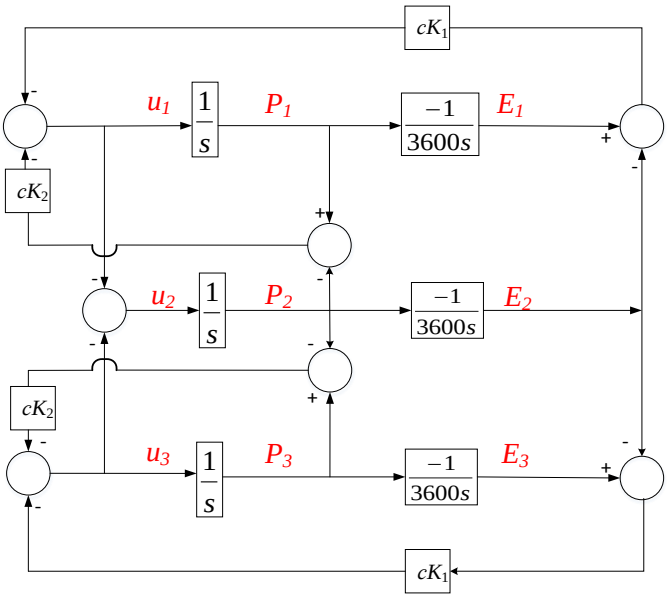

Fig. 2. Block diagram of the simplified battery models including consensus based SoC management control.

Fig. 2 shows the block diagram of the communication system shown in Fig. 1 with simplified dynamic models of the batteries in (4) and consensus control inputs in (14). The combined system can provide a clear idea about how the proposed algorithm can synchronize the energy levels of each battery energy storage unit.

a) Design considerations: Fig. 3 shows a sample design by choosing a set of Q and R. The resulting system dynamics show that Battery 1's power may increase 50% due to its high SoC. Battery 3's power is reduced to almost zero. In real-world scenarios, a battery power is limited. It is also not desirable to have batteries operating in different modes, with some charging and some discharging. Fig. 4 shows a different set of parameters (values of Q decreased and R increases) which leads to less overshoot of power and longer convergence time.

The main step in selecting the parameters is to select Q and R. Then K will be derived based on equation (8). Generally, Q and R should firstly be selected as positive definite matrices and satisfy the condition (9) where P_1 is positive definite.

b) Sensitivity of the parameters: Q is the weight matrix related to state x_i and R is the weight matrix related to input u_i. A larger Q results in faster dynamic response in x_i while a larger R penalizes the input and results in less effort in control or small values in u_i. Case 1 (Fig. 3) shows a faster consensus dynamics due to faster dynamic responses of individual agents compared to Case 2 (Fig. 4).

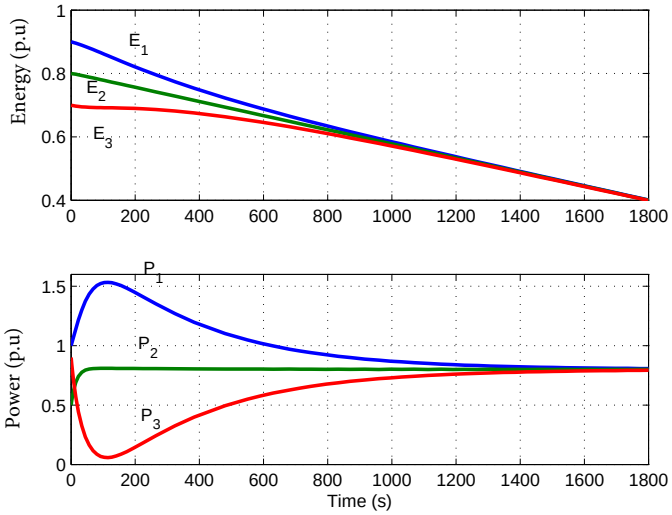

Fig. 3. Simulation results of the analysis model. $Q = diag([800, 10]), R = 200, K_1 = -20, K_2 = 2.23860, c = 0.01$.

While tuning the gains, one should consider that improving the convergence may result in overshoots. Therefore, there should be a balance between convergence time and overshoots in power order. For example, in Case 1 (Fig. 3), the overshoot in power order is high (about 50%), but the convergence is achieved in 1400 seconds. In comparison, convergence is longer in Case 2 (about 1800 seconds) but the overshoot in power order is less than 20% (Fig. 4). Both designs are tested when the power limit of 1 p.u is enforced. Fig. 5 shows the comparison for two different designs shown in Fig. 3 and Fig. 4. It is obvious that Design 2 leads to a more desirable performance. Design 1 will lead to different operation modes for batteries. One battery will work in charging mode while the other two will work in discharging mode.

III. Consensus Control Validation using High-Fidelity Testbed

A. Test system circuit configuration

The first system to be investigated is a 14-bus microgrid model composed of three detailed battery modules with parallel adjustable loads, and an induction machine. The entire system may be connected to the main ac grid through a transmission line and a breaker. Such a system is illustrated in Fig. 6. Each inverter has the capability to be connected to the grid and perform the independent active and reactive power control as well. In islanded microgrid operation, the battery inverters function to retain the voltage and frequency. Detailed parameters of the system are provided in the Appendix.

B. Detailed Battery Models

Several battery models have been proposed so far. Among all, electrical models are more accurate and provide more balance between electrochemical and mathematical models. Electrical models are composed of voltage sources, resistors, and capacitors which are the best options for co-simulations. There are several electrical models such as: impedance based,

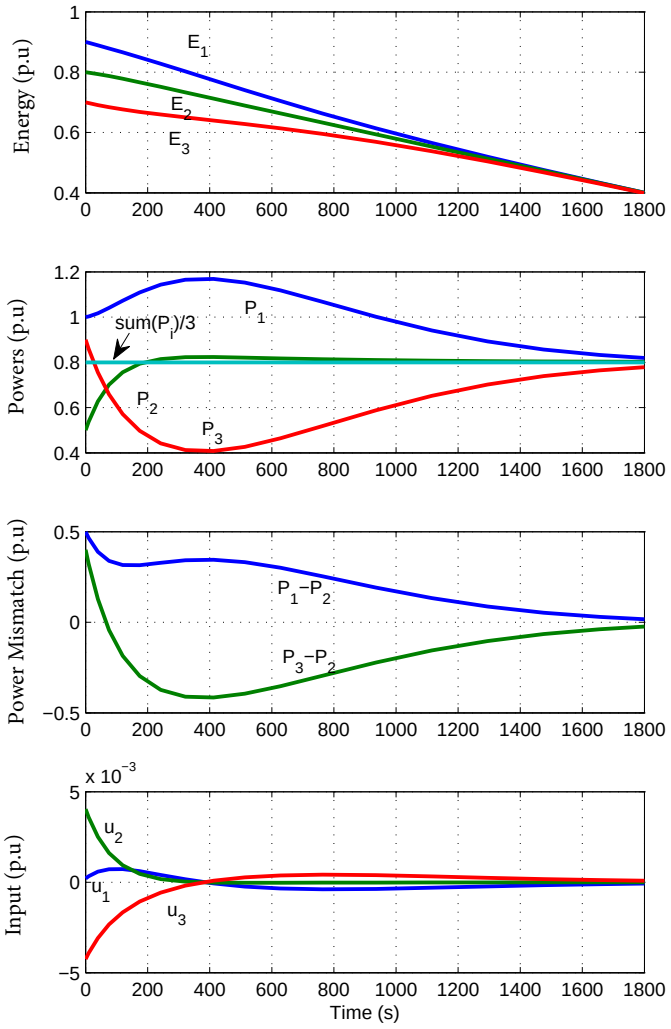

Fig. 4. Simulation results of the analysis model. $Q = diag([300, 10]), R = 5000, K_1 = -2.4495$, $K_2 = 0.4487$, $c = 0.01$.

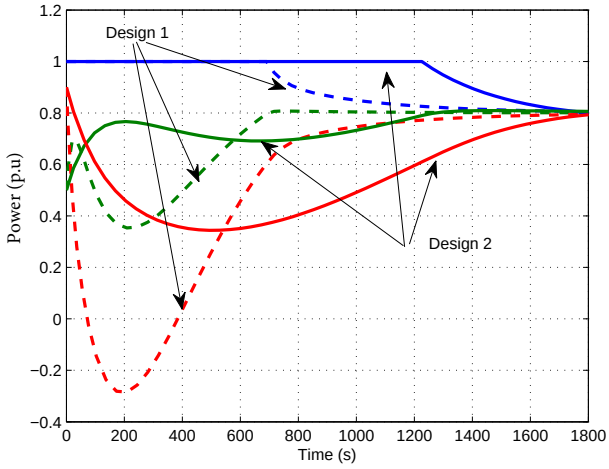

Fig. 5. Comparison of two designs when power limits are enforced.

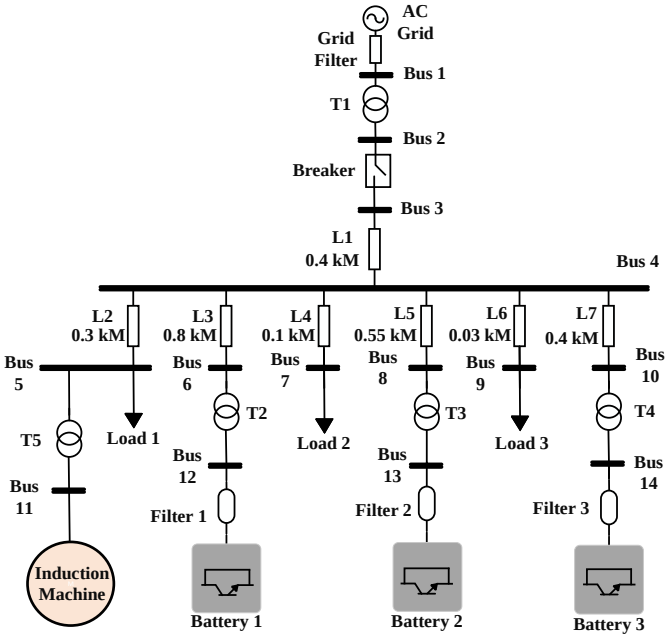

Fig. 6. Microgrid system composed of battery energy storage systems and loads. The battery voltage level is 400 V and the grid voltage is 13.8 kV. The battery size is 100 kW/200 kWh. Transmission lines have the same impedance of $0.0825 + j0.284\Omega/kM$.

Thevenin based, and run-time based [29]. The model developed in [10] is adopted in this research. The designed approach provides an accurate electrical model with transient and steady state dynamic response. Such a model is illustrated in Fig. 7.

In this study, each battery is designed for 100 kW base power and is chosen to be the Li-ion type. The capacity of the battery in Farad (C_c), which defines the full capacity when it is fully charged, is expressed by :

$$C_c = 3600 \frac{P_n . f_1 . f_2}{V_n} \tag{15}$$

where P_n is the nominal energy of the battery in Whr, V_n is the nominal battery voltage, f_1 and f_2 are correction factors. Parameters of the battery then can be derived by [10]:

$$\begin{aligned} V_{SOC} &= -1.03e^{-35SoC} + 3.6 + 0.2SoC - 0.1SoC^2 + 0.3SoC^3 \\ R_s &= 0.1562e^{-24.37SoC} + 0.07446 \\ R_{TS} &= 0.3208e^{-29.14SoC} + 0.04669 \\ C_{TS} &= -752.9e^{-13.51SoC} + 703.6 \\ R_{TL} &= 6.603e^{-155.2SoC} + 0.04984 \\ C_{TL} &= -6065e^{-27.12SoC} + 4475 \end{aligned} \tag{16}$$

where R_{SD} is the self discharge resistor, R_{TS} is the short transient resistor, R_s is the series resistor, and R_{TL} is the long transient resistor. C_{TS} and C_{TL} are short and long transient capacitors. In this study, P_n is set to 200 kWh and V_n is set to 400 V. The detailed battery model is then connected to an inverter to convert the dc signals to ac. The parameters for the mentioned battery are included in the Table I.

C. Battery converter controls

The converter control blocks are shown in Fig. 8, including inner current control, power following control, voltage controller, primary frequency control and secondary frequency control. The consensus control input is notated as u_i in Fig.

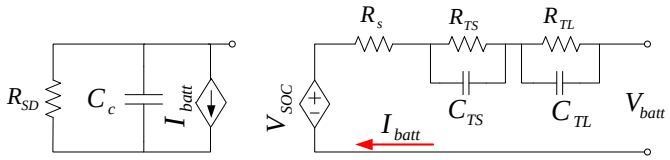

Fig. 7. Detailed electrical battery model.

TABLE I
PARAMETERS OF INDIVIDUAL BATTERIES

Quantity	Value
R_{DS}	$1e^6$ Ω
C_C	$39e^5$ F
R_S	0.0074 Ω
R_{TS}	0.0046 Ω
C_{TS}	$70.36e^3$ F
R_{TL}	0.0498 Ω
C_{TL}	$447.5e^3F$
f_1, f_2	1

8. This signal combined with the frequency deviation will be fed into an integrator to generate power orders.

The inner current loops are in charge of generating reference voltages in dq frame based on input reference currents in dq frame. The feed-forward items v_{fd} and v_{fq} are the point of common coupling (PCC) voltage measured in the dq frame and passed through a low pass filter to mitigate the unwanted harmonics from PCC voltage [30].

The next control level is power control Two PI controllers are used to force the steady state error to zero.

Primary frequency control is designed as primary droop control and the secondary frequency control will provide a frequency control in the case of dynamic events. Frequency and frequency deviation are measured by the PLL block. Primary voltage control may also be equipped for reactive power sharing.

In grid-connected mode, $\Delta\omega$ will be zero and frequency control loops will be deactivated. However, the consensus control inputs still will be activated which enables the energy management technique without deactivating the control loops.

The combined signal of consensus input and frequency deviation has a similar representation of area control error (ACE) signal employed in power systems for tie-line power scheduling and secondary frequency control. The parameters of the controllers are listed in Table II and Table III.

TABLE II
PARAMETERS OF CONTROLLERS

Control	Value
Inner current	k_{pi}=5, k_{ii}=100
Outer power	k_{pp}=0.1, k_{ip}=100
Secondary frequency	$k_{if1} = 0.01, k_{if2} = 0.02, k_{if3} = 0.04$
Primary frequency	$R_{f1} = 0.04, R_{f2} = 0.06, R_{f3} = 0.08$
Reactive droop	R_{q1}= 0.002, R_{q2}= 0.0025, R_{q3}= 0.0033

TABLE III
PARAMETERS OF BATTERY CONTROL

Quantity	Value
Switching frequency	1620 Hz
Inverter nominal power	100 kW
Low pass filter parameter, α_f	1000 Hz

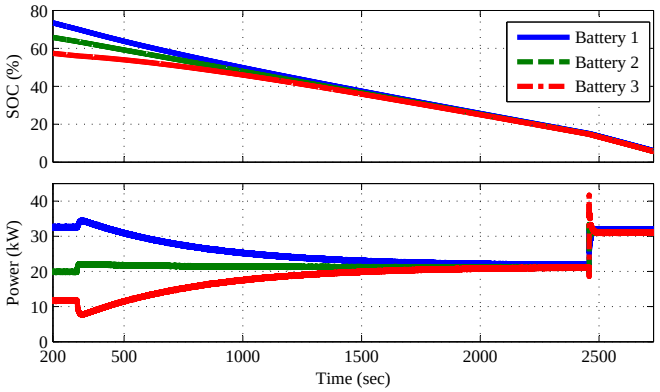

Fig. 9. Discharging case. Initial SOC and power levels for three batteries are different. Consensus control has been enabled at 300 seconds and consensus achieves at 2300 seconds. 30 kW load increase occurs at about 2458.5 seconds. The power levels achieve consensus at 2600 seconds, each 32 kW.

IV. RT-LAB SIMULATION RESULTS FOR 14-BUS MICROGRID

In this section, real-time simulations with RT-LAB are carried out to demonstrate the proposed controller. The main advantages of the real time simulators are: fast computing, real-time operation, and precision. By separating each simulation model into different subsystems, RT-LAB with multiple processing cores, will assign each subsystem to be compiled in a separate core. Therefore, the entire simulation can be run concurrently in multiple cores.

All the switching details of power electronic devices are included. This makes the results of real-time simulators close to reality. Two case studies are carried out: (1) a discharging case when the microgrid is in islanded mode, and (2) a charging case when the microgrid is in grid-connected mode.

TABLE IV
PARAMETERS OF THE SYSTEM

Quantity	Value
ac grid	13.8 kV, 60 Hz
Grid filter	0.1+j3 Ω
Filter 1	j0.6 Ω
Filter 2	j0.75 Ω
Filter 3	j0.9 Ω
Induction machine	5.5 kVA, 60 Hz, 0.4 kV
Load 1	33 kW
Load 2	20 kW, 5 kVAR
Load 3	13 kW

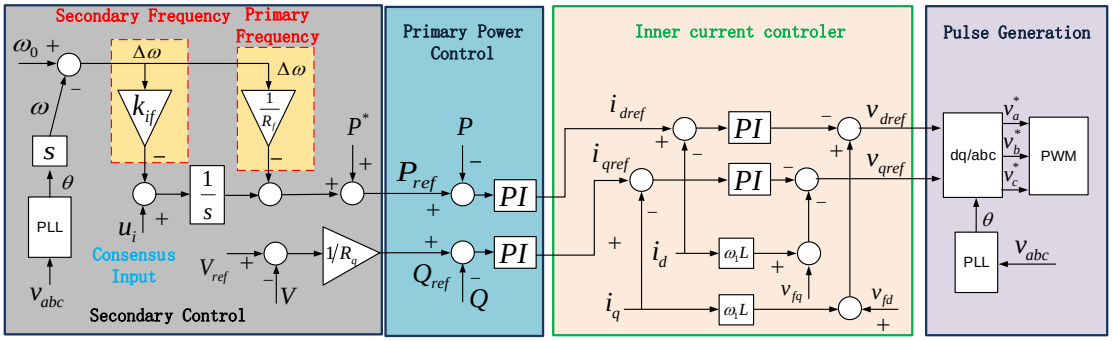

Fig. 8. Battery converter control blocks.

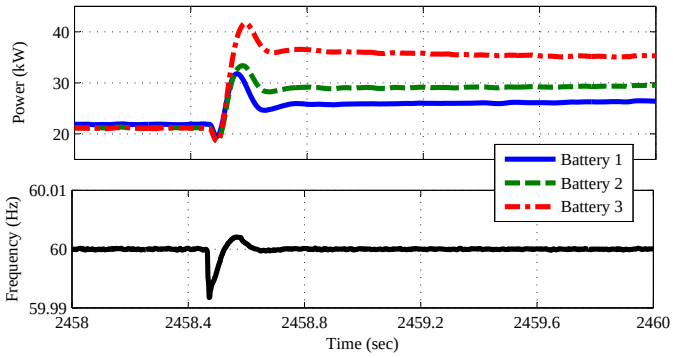

Fig. 10. Load increase occurs at 2458.5 seconds. Frequency is brought back to 60 Hz by secondary frequency control. The batteries power levels are different at 2458.5 seconds due to different gain for secondary frequency control: $K_{if1} = 0.01, K_{if2} = 0.02, K_{if3} = 0.04$.

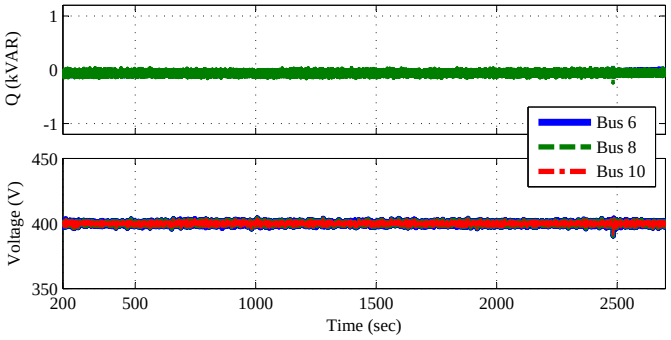

Fig. 11. Reactive power and voltage for three batteries; The reference reactive power is set to 0 and voltage reference is set to 400 V.

A. Discharging event - islanded mode

A discharging case is designed to test the performance of the designed consensus control in islanded mode. The energy storage should support the loads in this case. Initially, a 66 kW load is considered. The SoC and power levels of batteries are all different. The consensus control is enabled after 300 seconds. The consensus control parameters are $cK_1 = -0.0822, cK_2 = 0.042$. The SoC and power levels achieve consensus at 2300 seconds. At about 2458.5 seconds, a 30 kW load increase occurs and total load will be 96 kW. After the transient due to frequency control, SoC and power consensus again are achieved. Simulation results are shown in Figs. 9, 10 and 11. Fig. 10 shows the droop control capability right after the load change. It is observed that, initially, the batteries are scheduled based on their droop coefficient. Consensus will be achieved later as the consensus controller dynamics are slower. Fig. 11 shows that the controller does not have any adverse impact on the voltage/reactive power control loop and the voltage is controlled in islanded mode.

TABLE V
PARAMETERS OF TRANSFORMERS

Number	Voltage(kV)	Power(kVA)	Z_1,Z_2 (Ω)
T_1	13.8/0.4	800	0.02+j0.1
T_2 *to* T_5	0.4/0.4	200	0.01+j0.05

B. Charging event-grid connected mode

This case is designed to test the performance of the designed consensus control for a charging case. Simulation results for a charging event are illustrated in Fig. 12. The total charging power is 96 kW. Before the consensus control is enabled, each battery is charged at different power level. After the consensus control is enabled, SoC and power levels achieve consensus at 2500 seconds. The consensus control parameters are $cK_1 = -0.0513$ and $cK_2 = 0.018$.

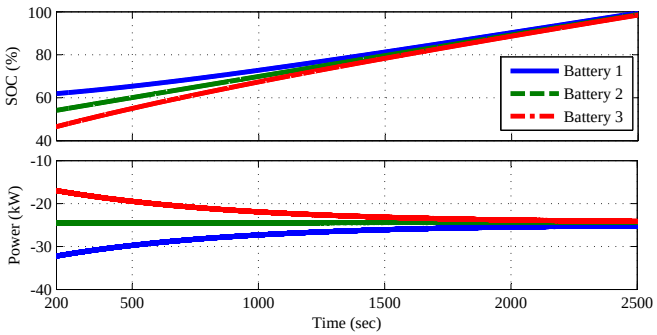

Fig. 12. A charging event shows power and SoC consensus are achieved after around 2500 seconds.

V. Simulation Results for IEEE 57-Bus Power System

To test the proposed algorithm in a larger power system case, a modified version of IEEE 57-bus test system has been considered. MatDyn [31], an open-source Matlab toolbox is adopted to carry out simulation. The original IEEE 57-bus system has 7 generators and 42 loads. To apply the proposed consensus algorithm into the system, the generators are replaced with the batteries as illustrated in Fig. 13.The simplified battery dynamics are considered for energy storage models and the consensus controller has been added to each battery based on the communication graph presented in Fig. 14.

Two case studies are considered:

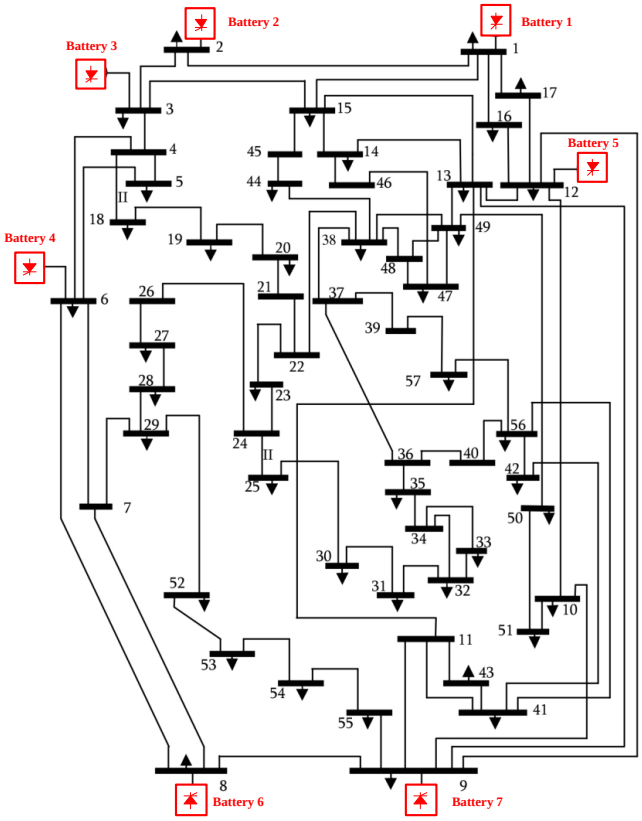

Fig. 13. Modified IEEE 57-bus case study.

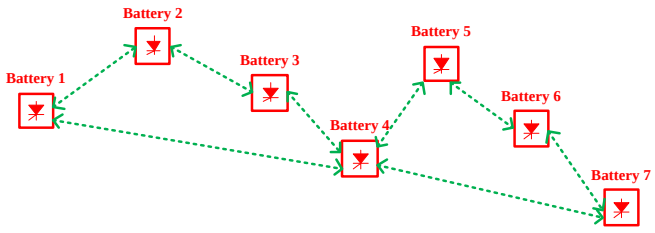

Fig. 14. Communication graph of the modified IEEE 57-bus case study.

- Case 1: no communication failure happens;
- Case 2: Battery 1 fails to communicate with the rest of the system.

Simulation results for the first case are shown in Fig. 15 (a) which shows the synchronization is achieved for all the energy storage devices. For case 2, battery 1 fails to communicate with the rest of the system.It is observed that, except the faulted battery, the rest of the system will synchronize successfully.

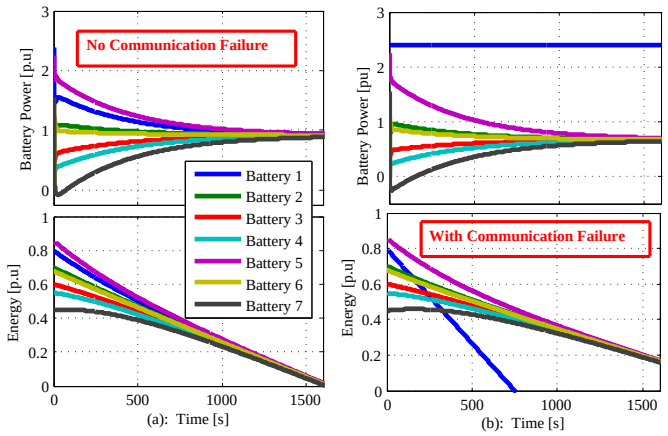

Fig. 15. Simulation results for consensus design for IEEE 57-bus power system. (a) Case 1: no communication failure; (b) Case 2: with communication failure at Bus 1.

VI. Conclusion

This paper applies consensus control to design battery coordination schemes. The design objective is to achieve SoC and power consensus regardless of charging, discharging or load varying operating modes. The main contribution is to treat battery SoC, power and the consensus control input as a double integrator system. The main assumption used in this design is (i) there is an integrator to generate power order, and (ii) the consensus dynamics are much slower than the rest of the system dynamics with primary and secondary control. Therefore, the assumption of the double integrator as the plant model is valid. This design philosophy renders an simple distributed control design with only SoC and power as exchange information.

The design is validated by RT-lab simulation for a high-fidelity 14-bus microgrid system with three batteries. To test the proposed design in a larger system, modified IEEE 57-bus power system with 7 batteries are also considered and two case studies are simulated. Simulation results show the effectiveness of the proposed consensus control.

Acknowledgement

The authors wish to acknowledge Prof. Lingling Fan's help on this research.

References

[1] S. Chiang, K. Chang, and C. Yen, "Residential photovoltaic energy storage system," *Industrial Electronics, IEEE Transactions on*, vol. 45, no. 3, pp. 385–394, 1998.

[2] J. Khazaei, Z. Miao, L. Piyasinghe, and L. Fan, "Real-time digital simulation-based modeling of a single-phase single-stage pv system," *Electric Power Systems Research*, vol. 123, pp. 85–91, 2015.

[3] L. Yazhou, "Studies on wind farm integration into power system," *Automation of Electric Power Systems*, vol. 8, p. 017, 2003.

[4] K. Divya and J. Østergaard, "Battery energy storage technology for power systems: An overview," *Electric Power Systems Research*, vol. 79, no. 4, pp. 511–520, 2009.

[5] X. Li, D. Hui, and X. Lai, "Battery energy storage station (bess)-based smoothing control of photovoltaic (pv) and wind power generation fluctuations," *Sustainable Energy, IEEE Transactions on*, vol. 4, no. 2, pp. 464–473, 2013.

[6] B. S. Borowy and Z. M. Salameh, "Dynamic response of a stand-alone wind energy conversion system with battery energy storage to a wind gust," *Energy Conversion, IEEE Transactions on*, vol. 12, no. 1, pp. 73–78, 1997.

[7] C. Hill, M. C. Such, D. Chen, J. Gonzalez, W. M. Grady *et al.*, "Battery energy storage for enabling integration of distributed solar power generation," *Smart Grid, IEEE Transactions on*, vol. 3, no. 2, pp. 850–857, 2012.

[8] J. M. Guerrero, J. C. Vasquez, J. Matas, D. Vicuna, L. García, and M. Castilla, "Hierarchical control of droop-controlled ac and dc microgrids: A general approach toward standardization," *Industrial Electronics, IEEE Transactions on*, vol. 58, no. 1, pp. 158–172, 2011.

[9] J.-Y. Kim, J.-H. Jeon, S.-K. Kim, C. Cho, J. H. Park, H.-M. Kim, and K.-Y. Nam, "Cooperative control strategy of energy storage system and microsources for stabilizing the microgrid during islanded operation," *Power Electronics, IEEE Transactions on*, vol. 25, no. 12, pp. 3037–3048, 2010.

[10] Z. Miao, L. Xu, V. R. Disfani, and L. Fan, "An soc-based battery management system for microgrids," *Smart Grid, IEEE Transactions on*, vol. 5, no. 2, pp. 966–973, 2014.

[11] X. Lu, K. Sun, J. M. Guerrero, J. C. Vasquez, L. Huang, and R. Teodorescu, "Soc-based droop method for distributed energy storage in dc microgrid applications," in *Industrial Electronics (ISIE), 2012 IEEE International Symposium on*. IEEE, 2012, pp. 1640–1645.

[12] X. Lu, K. Sun, J. M. Guerrero, J. C. Vasquez, and L. Huang, "State-of-charge balance using adaptive droop control for distributed energy storage systems in dc microgrid applications," *Industrial Electronics, IEEE Transactions on*, vol. 61, no. 6, pp. 2804–2815, 2014.

[13] R. M. Murray and R. Olfati-Saber, "Consensus protocols for networks of dynamic agents," *IEEE Proceedings, American Controls Conference*, 2003.

[14] D. P. Spanos, R. Olfati-Saber, and R. M. Murray, "Dynamic consensus on mobile networks," *IFAC world congress*, pp. 1–6, 2005.

[15] B. Tordoff and D. W. Murray, "Guided sampling and consensus for motion estimation," *European conference on computer vision*, pp. 82–96, 2002.

[16] Z. Zhang and M.-Y. Chow, "Convergence analysis of the incremental cost consensus algorithm under different communication network topologies in a smart grid," *IEEE Transactions on Power Systems*, vol. 27, no. 4, pp. 1761–1768, 2012.

[17] G. Binetti, A. Davoudi, F. L. Lewis, D. Naso, and B. Turchiano, "Distributed consensus-based economic dispatch with transmission losses," *IEEE Transactions on Power Systems*, vol. 29, no. 4, pp. 1711–1720, 2014.

[18] S. Yang, S. Tan, and J.-X. Xu, "Consensus based approach for economic dispatch problem in a smart grid," *IEEE Transactions on Power Systems*, vol. 28, no. 4, pp. 4416–4426, 2013.

[19] F. Guo, C. Wen, J. Mao, and Y.-D. Song, "Distributed secondary voltage and frequency restoration control of droop-controlled inverter-based microgrids," *Industrial Electronics, IEEE Transactions on*, vol. 62, no. 7, pp. 4355–4364, 2015.

[20] A. Bidram, A. Davoudi, F. L. Lewis, and J. M. Guerrero, "Distributed cooperative secondary control of microgrids using feedback linearization," *Power Systems, IEEE Transactions on*, vol. 28, no. 3, pp. 3462–3470, 2013.

[21] L.-Y. Lu and C.-C. Chu, "Consensus-based droop control synthesis for multiple dics in isolated micro-grids," *Power Systems, IEEE Transactions on*, vol. 30, no. 5, pp. 2243–2256, 2015.

[22] J. Schiffer, T. Seel, J. Raisch, and T. Sezi, "Voltage stability and reactive power sharing in inverter-based microgrids with consensus-based distributed voltage control," *Control System Technology, IEEE Transactions on*, vol. 24, no. 1, pp. 96–109, 2015.

[23] T. Morstyn, B. Hredzak, and V. G. Agelidis, "Distributed cooperative control of microgrid storage," *Power Systems, IEEE Transactions on*, vol. 30, no. 5, pp. 2780–2789, 2015.

[24] ——, "Communication delay robustness for multi-agent state of charge balancing between distributed ac microgrid storage systems," in *2015 IEEE Conference on Control Applications (CCA)*, Sept 2015, pp. 181–186.

[25] C. Li, T. Dragicevic, J. C. Vasquez, J. M. Guerrero, and E. A. A. Coelho, "Multi-agent-based distributed state of charge balancing control for distributed energy storage units in ac microgrids," in *2015 IEEE Applied Power Electronics Conference and Exposition (APEC)*, March 2015, pp. 2967–2973.

[26] H. Zhang, F. L. Lewis, and Z. Qu, "Lyapunov, adaptive, and optimal design techniques for cooperative systems on directed communication graphs," *Industrial Electronics, IEEE Transactions on*, vol. 59, no. 7, pp. 3026–3041, 2012.

[27] J. A. Fax and R. M. Murray, "Information flow and cooperative control of vehicle formations," *Automatic Control, IEEE Transactions on*, vol. 49, no. 9, pp. 1465–1476, 2004.

[28] F. L. Lewis, H. Zhang, K. Hengster-Movric, and A. Das, *Cooperative control of multi-agent systems: optimal and adaptive design approaches*. Springer Science & Business Media, 2013.

[29] M. Chen, G. Rincón-Mora *et al.*, "Accurate electrical battery model capable of predicting runtime and iv performance," *Energy Conversion, IEEE Transactions on*, vol. 21, no. 2, pp. 504–511, 2006.

[30] L. Harnefors, M. Bongiorno, and S. Lundberg, "Input-admittance calculation and shaping for controlled voltage-source converters," *Industrial Electronics, IEEE Transactions on*, vol. 54, no. 6, pp. 3323–3334, 2007.

[31] S. Cole and R. Belmans, "Matdyn, a new matlab-based toolbox for power system dynamic simulation," *IEEE Transactions on Power systems*, vol. 26, no. 3, pp. 1129–1136, 2011.

Javad Khazaei (S'10 M'16) received his Bachelor's degree in Electrical Engineering from Mazandaran University (2009) and Master's degree from Urmia University (2011) in Iran. He received his Ph.D degree at University of South Florida (USF) in Summer 2016. He is currently an Assistnat Professor at Penn State Harrisburg. His research interests include Microgrid modeling, Renewable Energy Integration, and Power Electronics applications.

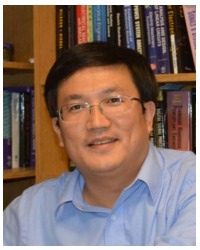

Zhixin Miao (S'00 M'03 SM'09) received the B.S.E.E. degree from the Huazhong University of Science and Technology,Wuhan, China, in 1992, the M.S.E.E. degree from the Graduate School, Nanjing Automation Research Institute, Nanjing, China, in 1997, and the Ph.D. degree in electrical engineering from West Virginia University, Morgantown, in 2002.

Currently, he is with the University of South Florida (USF), Tampa. Prior to joining USF in 2009, he was with the Transmission Asset Management Department with Midwest ISO, St. Paul, MN, from 2002 to 2009. His research interests include power system stability, microgrid, and renewable energy.